Exciton-phonon effects in carbon nanotube optical absorption

Vasili Perebeinos, J. Tersoff, and Phaedon Avouris*
IBM Research Division, T. J. Watson Research Center, Yorktown Heights, New York 10598
(Dated: November 1, 2004)

We find that the optical properties of carbon nanotubes reflect remarkably strong effects of exciton-phonon coupling. Tight-binding calculations show that a significant fraction of the spectral weight of the absorption peak is transferred to an exciton+phonon sideband, which is peaked at around 200 meV above the main absorption peak. The exciton-phonon coupling is reflected in a dynamical structural distortion, which contributes a binding energy of up to 100 meV. The distortion is surprisingly long-ranged, and is strongly dependent on chirality.

PACS numbers: 78.67.Ch,71.10.Li,71.35.Cc

The optical properties of carbon nanotubes are currently the focus of intense experimental and theoretical attention [1–12], and even single nanotube electro-optical devices have been demonstrated [13–15]. While most of the experimental results have been discussed in terms of intraband transitions, a number of calculations have found strong electron-hole interactions that lead to the formation of excitons [7–12]. New information has been obtained from recent photoconductivity excitation spectra [16, 17] that have revealed sidebands at about 200 meV above to the main absorption peaks suggesting the involvement of phonons.

Here we present the first theoretical investigation of the role of electron-phonon coupling on the exciton and intraband spectra of carbon nanotubes. We find surprisingly strong effects on the excitonic spectra. While static electron-phonon effects are expected to be weak in nanotubes [18], we find that dynamical effects lead to the transfer of a significant fraction of the spectral weight from the exciton absorption peak (zero phonon line) to a phonon sideband peaked at around 200 meV (Fig. 1a), in agreement with the experimental observations. This finding supports the notion that the excited states of carbon nanotubes are indeed excitons. The fraction of the intensity transferred to the phonon sideband is inversely proportional to the nanotube diameter. The exciton-phonon binding energy is also unexpectedly high, about 60-100 meV. The associate lattice distortions exhibit an intriguing structure, extend far beyond the exciton size itself [11] and reverse sign for different nanotube chiralities (Fig. 1b-c). The effect of the changing the dielectric environment on the spectra is also discussed.

In the absence of exciton-phonon coupling, emission or absorption of a photon involves an exciton of total wavevector q_ϕ corresponding to the photon momentum, hereafter approximated as $q_\phi = 0$. The exciton-phonon coupling mixes this exciton with phonons and with excitons of other q, such that the total exciton+phonon momentum is conserved.

The finite-q exciton wavefunction can be found from the solution of the Bethe-Salpeter Equation (BSE) [19] in the basis of a tight-binding Hamiltonian [20], analogous to the case with $q = 0$ considered in [11]:

$$\left|\Psi_q^S\right\rangle = \sum_k A_{kq}^S u_{k+q}^\dagger v_k \left|\mathrm{GS}\right\rangle . \quad (1)$$

Here A_{kq}^S is the eigenvector of the S's state of BSE solution; $u_{k+q}^\dagger$ (v_k) creation (annihilation) of an electron in the conduction (valence) band acting on the ground state $|\mathrm{GS}\rangle = \prod_k v_k^\dagger |\mathrm{vac}\rangle$. The indices k and q label the continuous 1D wavevector along the tube axis and the discrete wavevector around the tube circumferences (the band index), respectively.

We model the electron-phonon interaction by the Su-Schrieffer-Heeger (SSH) model [21], with matrix element $t = t_0 - g\delta u$ dependent on the change of the nearest neighbor C-C distance (δu), where $t_0 = 3$ eV. We take the electron-phonon coupling constant to be $g = 5.3$ eV/Å as predicted theoretically for a related molecular problem [22], consistent with fits to the Peierls gap in conjugated polymers [23].

After Fourier transformation the intraband SSH Hamiltonian has the form:

$$\mathcal{H}_{\mathrm{el-ph}} = \sum_{kq\mu} \mathrm{M}_{kq}^\mu (v_{k+q}^\dagger v_k - u_{k+q}^\dagger u_k)(a_{q\mu} + a_{-q\mu}^\dagger), \quad (2)$$

where $\mathrm{M}_{kq}^\mu \propto gN^{-1/2}$ is momentum dependent electron-phonon coupling; $a_{-q\mu}^\dagger$ is a phonon creation operator with wavevector $-q$ and phonon band index $\mu = 1...6$; and N is the number of primitive unit cells, each containing two carbons. For the phonon spectrum we used a force-constant model similar to Saito *et al.* [24].

The electron-phonon Hamiltonian mixes the optically active q=0 exciton with finite-q excitons in combination with phonons of wavevector $-q$:

$$\begin{aligned} \mathcal{H}_{\mathrm{el-ph}} \left|\Psi_0^S\right\rangle &= -\sum_{S'q\mu} B_{q\mu}^{SS'} a_{-q\mu}^\dagger \left|\Psi_q^{S'}\right\rangle \\ B_{q\mu}^{SS'} &= \sum_k \mathrm{M}_{kq}^\mu A_{kq}^{S'*} (A_{k,0}^S + A_{k+q,0}^S) \end{aligned} \quad (3)$$

Here the orthogonality relation of the BSE solution ($\sum_S A_{kq}^S A_{k'q}^{S*} = \delta_{kk'}$) has been used to derive exciton-phonon coupling amplitudes $B_{q\mu}^{SS'}$.

The wavefunction and the spectral line shape can be evaluated in second order perturbation theory for the lowest optically active exciton s:

$$\left|\tilde{\Psi}_0^s\right\rangle \propto |\Psi_0^s\rangle + \sum_{qS'\mu} \frac{B_{q\mu}^{sS'}}{E_q^{S'} + \hbar\omega_{-q\mu} - E_0^s} a_{-q\mu}^\dagger \left|\Psi_q^{S'}\right\rangle$$

$$I(\omega) \propto \delta(E_0^s - \hbar\omega) + \sum_{qS'\mu} \frac{\left|B_{q\mu}^{sS'}\right|^2}{(E_q^{S'} + \hbar\omega_{-q\mu} - E_0^s)^2} \times\delta(E_q^{S'} + \hbar\omega_{-q\mu} - \hbar\omega) \quad (4)$$

The absorption spectrum Eq. (4) is shown in Fig. 1a (solid red curve) for a (17,0) tube and $\varepsilon = 2$, where ε is the dielectric constant of the embedding medium [11]. Because of exciton-phonon coupling, the main absorption peak looses 8% of it's spectral weight to the sideband, which corresponds to the continuum of finite-q excitons plus phonon of wavevector $-q$. Most of the transferred spectral weight goes to the prominent sideband at about 210 meV above the zero phonon line, with 4% of the spectral weight falling between 100 and 300 meV. The SSH Hamiltonian has little coupling to the low frequency modes and we find a much weaker replica at the breathing mode frequency [i.e. 20 meV for a (17,0) tube].

To analyze the sideband in more detail, we recalculate the sideband spectra in the interval $0.1\text{eV} \leq E_q^{S'} + \hbar\omega_{-q\mu} - E_0^s \leq 0.3\text{eV}$ neglecting either exciton or phonon dispersion. [We do this by setting $E_q^{S'} = E_0^s$ or $\hbar\omega_{-q\mu} = 0$ in delta-function arguments in Eq. (4).] The results are shown by the dashed and dotted lines respectively in Fig. 1a. The phonon contribution to the sideband peak consists of two peaks, corresponding to the phonon band edges at 175 meV and 198 meV, the latter being much weaker. The energy difference between the sideband peak position and optical phonon frequency is due to the exciton "recoil energy", i.e. the energy from finite q-exciton, which contributes ∼30 meV here.

In the presence of an exciton the nanotube distorts dynamically. While the electron remains within roughly 2 nm of the hole for the cases shown in Fig. 1, the structural distortions are far more long-ranged. The distortions calculated using the wavefunction Eq. (1) are shown in Fig. 1b and 1c for (16,0) and (17,0) tubes respectively, plotting the atomic displacements relative to the position of the hole. The breathing distortions decay exponentially away from the exciton, with a decay length of $\lambda_b = 13$ nm. We find that λ_b is proportional to the tube diameter. The sign of the breathing distortion depends on chirality indices (n,m): positive for mod(n-m,3)=1 and negative for mod(n-m,3)=2. From the sign of the exciton-phonon matrix elements, we expect a reversal of the signs of the breathing distortions for the second exciton. The displacements parallel to the tube axis decay far more slowly even than this, oscillating with a wavevector $\lambda_z \approx 80$ nm, which appears to be independent of the tube

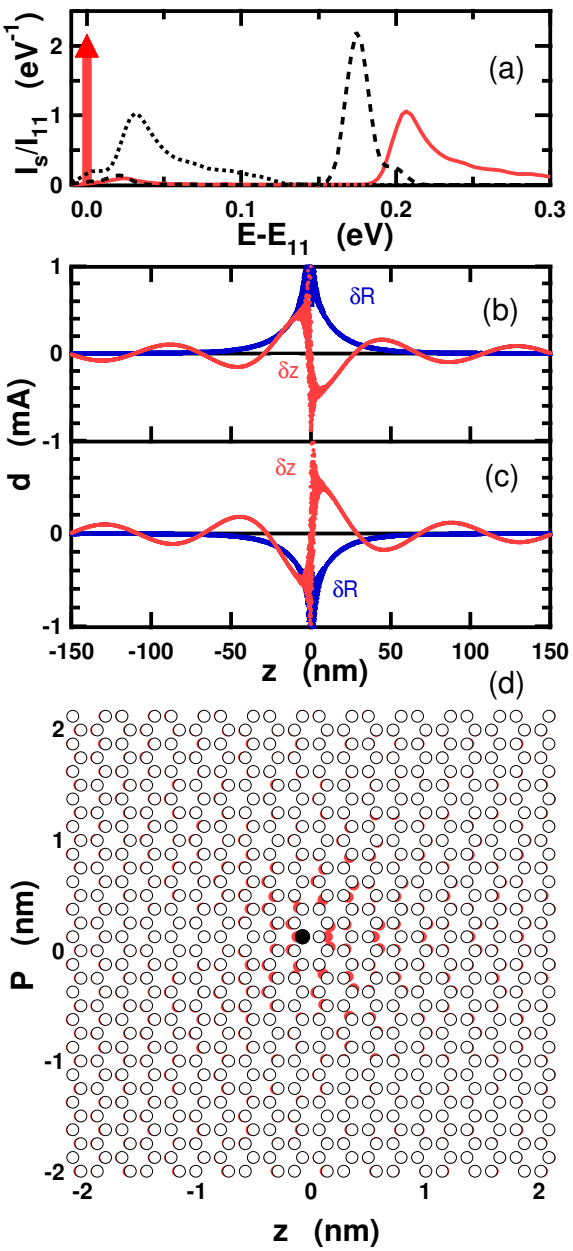

FIG. 1: (color online). (a) Absorption spectrum Eq. (4) for (17,0) tube and $\varepsilon = 2$ (solid red curve and red delta-function); dashed and dotted lines show respectively the phonon and exciton contributions to the sideband energy, as described in text. (b) Long-range tail of the atomic displacements with respect to the hole position (at origin) for a (16,0) tube: radial displacements (labeled δR, in blue), and displacements parallel to the axis (labeled δz, in red). (c) Same for (17,0) tube. (d) Short-range azimuthal and axial distortions, shown on "unwrapped" carbon nanotube by displaying the displaced atom positions (red circles) together with undisplaced positions (white circles), with displacements magnified by a factor of 230 for visibility. Hole position is solid circle at center.

diameter. The short-range distortions near the exciton are shown in Fig. 1d.

The spectra for higher-energy excitons ($E_0^S > E_0^s$) cannot be obtained from Eq. (4), because the denominator $E_q^{S'} + \hbar\omega_{-q\mu} - E_0^S$ can be arbitrarily close to zero and the perturbation theory breaks down. Toyozawa showed [25] that an exact solution for the absorption spectra has a form similar to the perturbation theory expression, with an energy dependent lifetime and polaronic shift in the energy denominator. We approximate Toyozawa's solution by evaluating the lifetime broadening in the Random Phase Approximation (RPA):

$$I(\omega) = \sum_S \frac{f_S}{\pi} \frac{\Gamma_S(\omega)}{(\hbar\omega - E_0^S)^2 + \Gamma_S(\omega)^2}$$
$$\Gamma_S(\omega) = \pi \sum_{S'q\mu} \left| B_{q\mu}^{SS'} \right|^2 \delta(\hbar\omega - E_q^{S'} - \hbar\omega_{-q\mu}), \quad (5)$$

where f_S is the oscillator strength of the S exciton [11]. We checked that the Toyozawa solution obtained with a self consistent Born approximation neglecting the k dependence of the self energy $\Sigma_S(E) = \Delta_S(E) + \Gamma_S(E)$ does not change the RPA result Eq. (5). If $\hbar\omega = E_0^S$ in Eq. (5) then $\Gamma_S(E_0^S)/\hbar$ equals half of the reciprocal lifetime of S-exciton due to the scattering by phonons. The binding energy shift for the S-exciton in RPA approximation is:

$$\delta E_S = \sum_{S'q\mu} \left| B_{q\mu}^{SS'} \right|^2 \mathcal{P}(E_0^S - E_q^{S'} - \hbar\omega_{-q\mu})^{-1}, \quad (6)$$

where $\mathcal{P}$ denotes the principle part.

The absorption spectra calculated with and without exciton-phonon coupling are shown in Fig. 2 for the tube embedded in dielectric $\varepsilon = 2$, 4, and for the free electron-hole pair absorption (equivalent to the limit $\varepsilon \to \infty$). In the absence of exciton-phonon interactions there are two strong exciton absorption peaks, each followed by the corresponding continuum of intraband absorption [11]. The first exciton has zero width in this approximation, and is shown by a vertical arrow in Fig. 2a and 2b. The second exciton can decay into the free electron-hole pairs of the first band via Coulomb interaction or by emitting a phonon, giving rise to a finite lifetime of the second exciton resonance. The actual value of the lifetime is very sensitive to the lineup of the resonance peak position with the onset of the first band continuum; the electronic and phonon contributions are given in the figure caption for a (17,0) tube for two values of ε. The sideband structure for the first exciton is similar to the perturbation theory result, and a sideband peak at around 200 meV is also predicted for the second exciton in the full calculation.

We decompose the sideband spectra into phonon and exciton-dispersion contributions in Fig. 3, as for Fig. 1a. The sideband spectra (solid lines) in Fig. 3 are the same

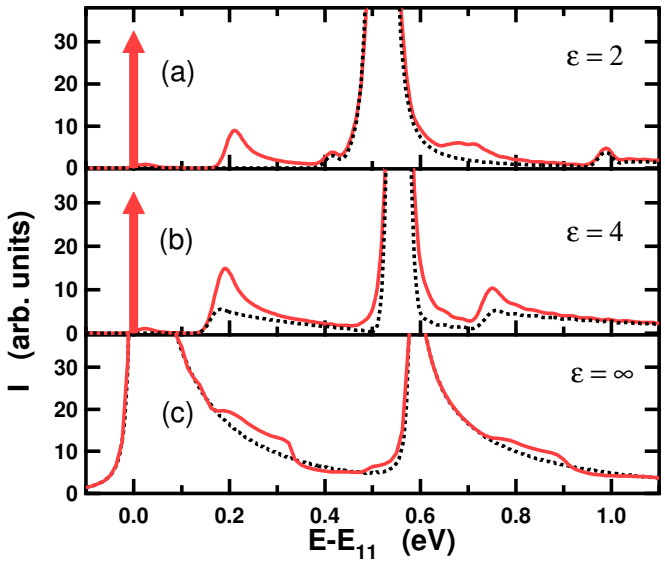

FIG. 2: (color online). Absorption spectra in (17,0) tube calculated with and without electron-phonon couplings (solid red and dashed black curves respectively) for (a) $\varepsilon = 2$, (b) $\varepsilon = 4$, (c) $\varepsilon \to \infty$. The zero of energy corresponds to the onset of the first optically active exciton, which has zero width and is shown by the vertical arrows. The width of the second exciton is finite due to: (1) coupling with the first band electron-hole continuum to give lifetimes of τ_{ee}=10 fs and 15 fs for ε =2 and 4 respectively; and (2) coupling with phonons to give τ_{ph}=90 fs and 33 fs for ε =2 and 4 respectively. Delta functions in Eq. (4) were Gaussian broadened with width of 20 meV.

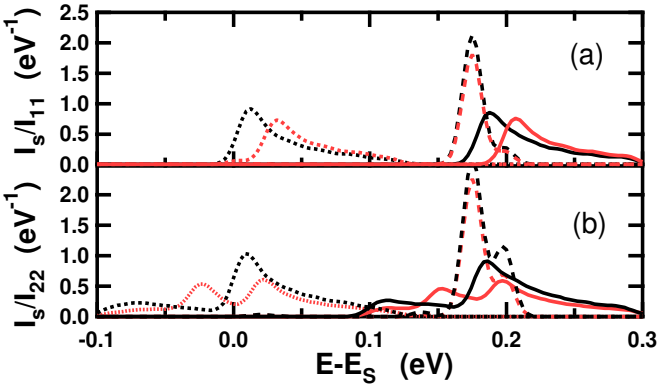

FIG. 3: (color online). Relative sideband intensity in the interval from 0.1 eV to 0.3 eV above the zero phonon line (solid curves), for $\varepsilon = 2$ (red) and $\varepsilon = 4$ (black). Dashed line is phonon contribution to sideband energy (calculated by neglecting exciton dispersion), and dotted line is exciton-dispersion ("recoil") contribution. (a) Sideband of first exciton, and (b) of second exciton. Delta functions were Gaussian broadened with width of 10 meV.

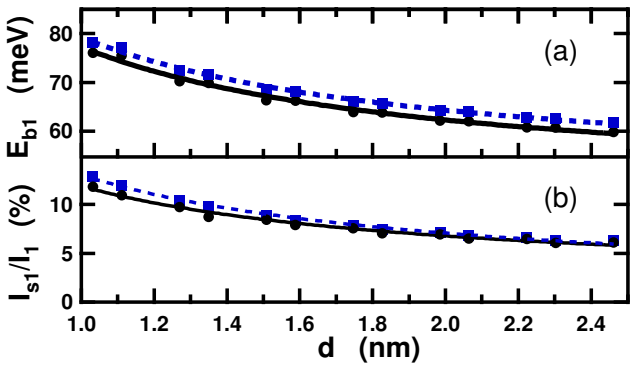

FIG. 4: (color online). (a) The phonon binding energy, and (b) fraction of the spectral weight transferred to the exciton+phonon sideband, for the first exciton in zig-zag tubes, versus tube diameter for $\varepsilon = 2$ (black circles) and for $\varepsilon = 4$ (blue squares) respectively. The curves (black solid for $\varepsilon = 2$ and blue dashed for $\varepsilon = 4$) are fits $A_{b,I} + B_{b,I}/d$, where $A_b = 47$ (meV), $B_b = 30$ (meVnm) and $A_I = 1.7$ (%), $B_I = 10$ (%nm) for $\varepsilon = 2$.

as in Fig. 2, except that Fig. 3 excludes the free electron-hole pair absorption contribution in order to focus exclusively on the exciton contribution. The phonon contributions for both excitons consist of two peaks centered at the optical phonon band edges, as in the perturbation theory result, independent of ε. On the other hand, the exciton contribution is different for the first and second excitons and depends on ε. The first exciton recoil energy is positive, and is smaller for larger ε. The second exciton recoil energy has both positive and negative contributions. The negative recoil energy is due to mixing of the second exciton with the first-band continuum. With larger ε the band mixing is reduced, which for the second exciton reduces in particular the negative recoil contribution. Thus for both excitons the structure of the phonon sideband is due to the exciton contribution, and is sensitive to the dielectric environment of the nanotube. The total spectral weights falling between 100 and 300 meV in the first and second sidebands are 3.6% and 5.3% for $\varepsilon = 2$ and 4.3% and 6.8% for $\varepsilon = 4$ respectively.

The total exciton binding energy calculated from Eq. (6) has the largest contribution from the coupling to the higher energy states, which have smaller optical spectral weight due to the second power of the energy difference $(E_q^{S'} + \hbar\omega_{-q\mu} - E_0^S)$ in the denominator of Eq. (5). The dependence of the binding energy on the diameter d is shown in Fig. 4a, along with a phenomenological fit, for the first exciton in different zig-zag tubes, for $\varepsilon = 2$ and 4. The second exciton binding energy is always larger than the first exciton, by 15-30%, due to the larger effective mass of the former. The fraction of the spectral weight transfer for the first exciton Eq. (4) is shown on Fig. 4b, along with a fit for the same values of ε.

In conclusion we have calculated the effect of the exciton-phonon interaction on the absorption spectra of carbon nanotubes in agreement with recent experiments [16, 17]. We predict a significant spectral weight transfer from the main absorption peak to a phonon sideband at around 200 meV above the zero phonon lines of the first and second excitons. We show that the environment-dependent "recoil" energy shifts and broadens the sideband peak and becomes responsible for the sideband lineshape. We also show that the second exciton recoil energy has both positive and negative contributions, due to band mixing, and that recoil effects are reduced with increasing ε. For the free electron-hole pair excitation (intraband transition) we find the phonon sideband peak to be smeared out due to the finite width of the van-Hove band excitation. We calculate a large exciton phonon binding of 60-100 meV which has a weaker ε dependence then the Coulomb binding energy. The fractional spectral-weight transfer and the binding energy both increase for small diameter tubes. The dynamical structural distortions are long-ranged and chirality dependent, such that tubes with mod(n-m,3)=1 stretch and tubes with mod(n-m,3)=2 shrink upon first exciton creation.

[*] Electronic address: avouris@us.ibm.com

[1] Z. M. Li, Z. K. Tang, H. J. Liu, N. Wang, C. T. Chan, R. Saito, S. Okada, G. D. Li, J. S. Chen, N. Nagasawa, and S. Tsuda, Phys. Rev. Lett. **87**, 127401 (2003).
[2] M. J. O'Connell, S. M. Bachilo, C. B. Huffman, V. C. Moore, M. S. Strano, E. H. Haroz, K. L. Rialon, P. J. Boul, W. H. Noon, C. Kittrell, J. Ma, R. H. Hauge, R. B. Weisman, and R. E. Smalley, Science, **297**, 593 (2002).
[3] S. M. Bachilo, M. S. Strano, C. Kittrell, R. H. Hauge, R. E. Smalley, R. B. Weisman, Science, **298**, 2361 (2002).
[4] A. Hagen and T. Hertel, Nano Lett. **3**, 383 (2003)
[5] S. Lebedkin, F. Hennrich, T. Skipa, and M. M. Kappes, J. Phys. Chem. B **107**, 1949 (2003).
[6] J. Lefebvre, Y. Homma, and P. Finnie, Phys. Rev. Lett.**90**, 217401 (2003)
[7] T. Ando, J. Phys. Soc. Japan **66**, 1066 (1996).
[8] T. G. Pedersen, Phys. Rev. B **67**, 073401 (2003).
[9] C.L. Kane and E. J. Mele, Phys. Rev. Lett. **90**, 207401 (2003).
[10] C. D. Spataru, S. Ismail-Beigi, L. X. Benedict, and S. G. Louie, Phys. Rev. Lett. **92**, 077402 (2004); Appl. Phys. A **78**, 1129 (2004).
[11] V. Perebeinos, J. Tersoff, Ph. Avouris, Phys. Rev. Lett. **92**, 257402 (2004).
[12] E. Chang, G. Bussi, A. Ruini, and E. Molinari, Phys. Rev. Lett. **92**, 196401 (2004).
[13] J. A. Misewich, R. Martel, Ph. Avouris, J. C. Tsang, S. Heinze, J. Tersoff, Science **300**, 783 (2003).
[14] M. Freitag, Y. Martin, J. A. Misewich, R. Martel, and Ph. Avouris, Nano Lett. **3**, 1067 (2003).
[15] M. Freitag, J. Chen, J. Tersoff, J. C. Tsang, Q. Fu, J. Liu, and Ph. Avouris Phys. Rev. Lett. **93**, 076803 (2004)
[16] Ph. Avouris, MRS Bulletin, **29**, 403 (2004).

[17] M. Freitag et al., to be published.
[18] J. W. Mintmire, B. I. Dunlap, and C. T. White, Phys. Rev. Lett. **68**, 631 (1992).
[19] M. Rohlfing and S. G. Louie, Phys. Rev. B **62**, 4927 (2000).
[20] R. Saito and H. Kataura, in *Carbon Nanotubes: Synthesis, Structure, Properties and Application*, edited by M. S. Dresselhaus, G. Dresselhaus, P. Avouris (Springer-Verlag, Heidelberg 2001), Vol. 80.
[21] W. P. Su, J. R. Schrieffer, and A. J. Heeger, Phys. Rev. Lett. **42**, 1698 (1979); Phys. Rev. B. **22**, 2099 (1980).
[22] V. Perebeinos, P. B. Allen, M. Pederson, cond-mat/0208051.
[23] R. Fincher et. al., Solid State Comm. **27**, 489 (1978).
[24] R. Saito *et al.*, Phys. Rev. B **57**, 4145 (1998).
[25] Y. Toyozawa, Prog. Theor. Phys. **20**, 53 (1958); J. Phys. Chem. Solids **25**, 59 (1964).